Energy-dependent multipole analysis for photoproduction of pions from protons

Alexander W. Smith and N. Zagury
Departamento de Física, Pontifícia Universidade Católica, Cx.P. 38071, Rio de Janeiro, RJ, Brasil
(Received 3 July 1979)

An energy-dependent multipole analysis for photoproduction of pions from protons from threshold up to 450 MeV is presented.

I. INTRODUCTION

The purpose of this paper is to present a semiphenomenological multipole analysis of pion photoproduction off protons in the region of the first π-N resonance.

Photoproduction of π^0 and π^+ around the first π-N resonance is reasonably well understood in terms of dispersion-relation models which were first introduced by Chew, Goldberger, Low, and Nambu (CGLN).[1] Although the main experimental results can be explained by these models, there are several uncertainties in the determination of the multipoles.

In the past years several semiphenomenological analysis[2-11] on photoproduction of pions off protons have appeared in the literature. In particular, Ref. 7 has presented an energy-dependent fit where the influence of nonuniformity of data-points distribution, in angle and energy, in the determination of the multipoles was studied.

This paper is an extension of Ref. 7. Besides analyzing a much larger set of data, we study the influence of nonuniformity of data distribution in angle, energy, and type of experiment. This is made through suitable weights associated to each data point.

In our approach, we take as first approximation a simple model and then ask for corrections, in the multipoles with $J \leq \frac{3}{2}$, that have an energy dependence which is the product of three factors: (i) a phase as given by the Fermi-Watson theorem,[12] (ii) threshold-behavior dependence, and (iii) a second-degree polynomial in the energy.

The multipoles with high angular momentum ($J > \frac{3}{2}$) will be fixed by the Born terms alone. As initial values for the multipoles, we will take the Born terms corrected for absorption except the resonant ones, which will be taken as $E_{1+}^{3/2}=0$ and $M_{1+}^{3/2}$ equal to the CGLN value.[1]

In Sec. II we review the kinematics and set the notation, in Sec. III we present the method, and in Sec. IV we discuss our results.

II. KINEMATICS

Let $\vec{k}$ and $\vec{q}$ be the photon and pion momenta in the center-of-mass system and θ the angle between them. Let $H_{\lambda,\mu}(\theta)$ be the helicity amplitude with labels corresponding to the final nucleon helicity λ and to the difference, μ, of the initial nucleon and the photon helicities. Although there are eight possible (λ, μ) pairs, parity conservation implies[13]

$$H_{\lambda,\mu}(\theta)=(-1)^{\lambda-\mu+1}H_{-\lambda,-\mu}(\theta) \tag{2.1}$$

reducing the number of independent amplitudes to four. Following Ecklund and Walker,[14] we call

$$\begin{aligned} H_1&= H_{1/2,3/2}= H_{-1/2,-3/2},\\ H_2&= H_{1/2,1/2}= -H_{-1/2,-1/2},\\ H_3&= H_{-1/2,3/2}= -H_{1/2,-3/2},\\ H_4&= H_{1/2,-1/2}= H_{-1/2,1/2}. \end{aligned} \tag{2.2}$$

In this analysis we will be concerned with four measurable quantities: the differential cross section $\sigma(\theta)$, the final nucleon polarization $P(\theta)$ in the $\vec{k}\times\vec{q}$ direction, the polarized-photon asymmetry $\Sigma(\theta)$, and the polarized-target asymmetry $T(\theta)$.

The expressions of these four quantities in terms of the helicity amplitudes[13] have been derived by several authors.[15] The differential cross section and the final nucleon polarization are given by

TABLE I. Distribution of the data analyzed in this paper.

	$\sigma(\theta)$	$P(\theta)$	$\Sigma(\theta)$	$T(\theta)$
π^+	1218	7	139	23
π^0	757	26	72	9
Total	1975	33	211	32

TABLE II. Distribution of data in intervals of angle and energy for case B.

(a) π^+ production

K_L (MeV) \ $\cos\theta$	−1	$-\frac{3}{4}$	$-\frac{2}{4}$	$-\frac{1}{4}$	0	$\frac{1}{4}$	$\frac{2}{4}$	$\frac{3}{4}$	1
150									
200	25	25	9	21	14	8	24	19	
250	39	31	21	32	16	24	32	31	
300	49	36	24	26	14	27	21	35	
350	62	46	29	32	11	34	29	53	
400	61	48	29	26	14	30	21	53	
450	43	40	23	18	14	22	15	31	

(b) π^0 production

K_L (MeV) \ $\cos\theta$	−1	$-\frac{3}{4}$	$-\frac{2}{4}$	$-\frac{1}{4}$	0	$\frac{1}{4}$	$\frac{2}{4}$	$\frac{3}{4}$	1
150									
200	7	11	6	17	6	4	3	2	
250	16	23	11	25	4	10	4	4	
300	33	33	23	37	15	17	5	6	
350	32	36	22	34	14	31	6	8	
400	20	37	26	34	18	28	10	17	
450	9	51	19	34	16	21	9	10	

TABLE III. Distribution of data in intervals of angle and energy for case C.

(a) π^+ production

K_L (MeV) \ $\cos\theta$	−1	$-\frac{2}{3}$	$-\frac{1}{3}$	0	$\frac{1}{3}$	$\frac{2}{3}$	1
150							
210	41	32	29	25	23	33	
270	65	37	47	27	35	56	
330	88	42	45	25	41	69	
390	98	61	44	23	40	77	
450	79	55	32	24	36	58	

(b) π^0 production

K_L (MeV) \ $\cos\theta$	−1	$-\frac{2}{3}$	$-\frac{1}{3}$	0	$\frac{1}{3}$	$\frac{2}{3}$	1
150							
210	16	21	22	8	8	5	
270	33	31	37	14	13	4	
330	51	48	55	27	23	9	
390	42	48	55	28	34	15	
450	31	57	49	30	30	20	

TABLE IV. Values for χ_W^2.

Solutions	χ_W^2
A	1.91
B	2.14
C	2.14
D	2.16
E	2.02

$$\sigma(\theta)=\frac{1}{2}\frac{q}{k}\sum_{i=1}^{4}|H_i|^2, \tag{2.3}$$

$$P(\theta)=-\frac{q}{k}\frac{1}{\sigma(\theta)}\mathrm{Im}(H_1H_3^*+H_2H_4^*). \tag{2.4}$$

The polarized-photon asymmetry Σ is defined as the ratio between the difference and the sum of the cross sections by photons linearly polarized in a direction perpendicular ($\sigma_\perp$) and parallel ($\sigma_\parallel$) to the plane of reaction:

$$\Sigma(\theta)=\frac{\sigma_\perp-\sigma_\parallel}{\sigma_\perp+\sigma_\parallel}=\frac{q}{k}\frac{1}{\sigma(\theta)}\mathrm{Re}(H_1H_4^*-H_2H_3^*). \tag{2.5}$$

The polarized-target asymmetry is defined as the ratio between the difference and sum of the cross

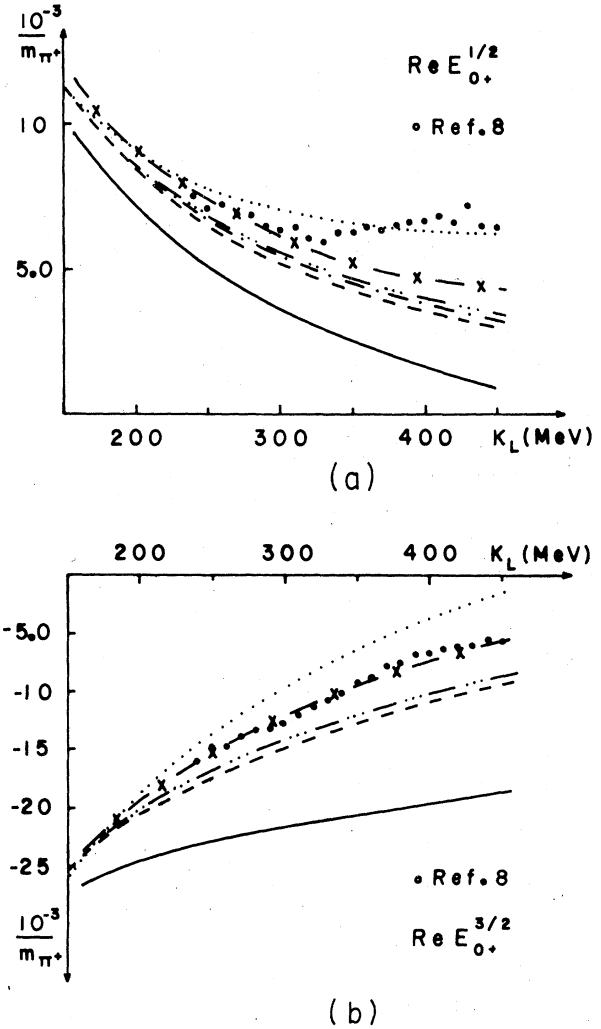

FIG. 1. (a) The real part of $E_{0+}^{1/2}$; (b) The real part of $E_{0+}^{3/2}$. The solid line is the input. The dashed line, the dotted line, the — ··· — line, the — · — line, and the —×— line correspond to solutions A, B, C, D, and E, respectively. For $E_{0+}^{3/2}$ the difference between solutions C and D is negligible and is not shown.

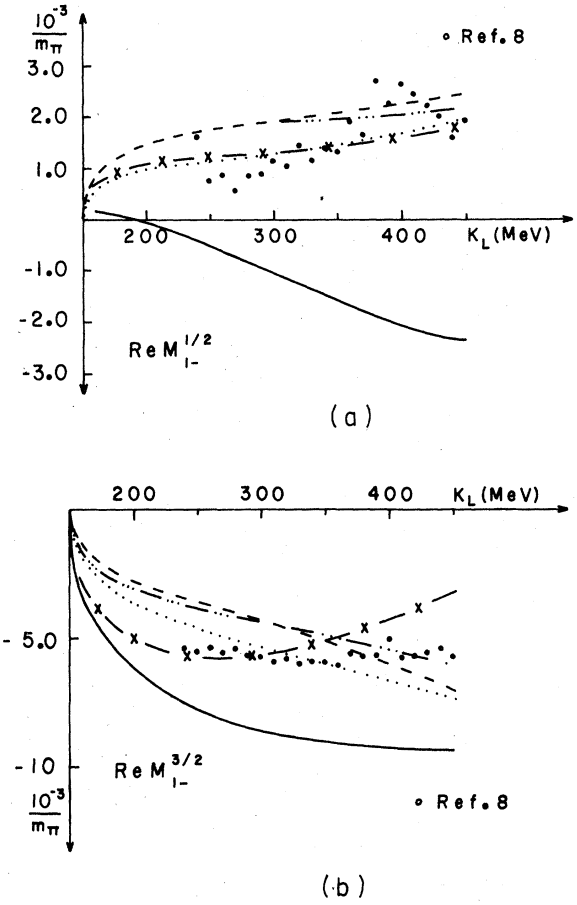

FIG. 2. (a) The real part of $M_{1-}^{1/2}$; (b) The real part of $M_{1-}^{3/2}$. The convention for the lines is the same of that in Fig. 1. For $M_{1-}^{1/2}$ the difference between solutions A and C is negligible and is not shown. For $M_{1-}^{3/2}$ the difference between solutions C and D is negligible and is not shown.

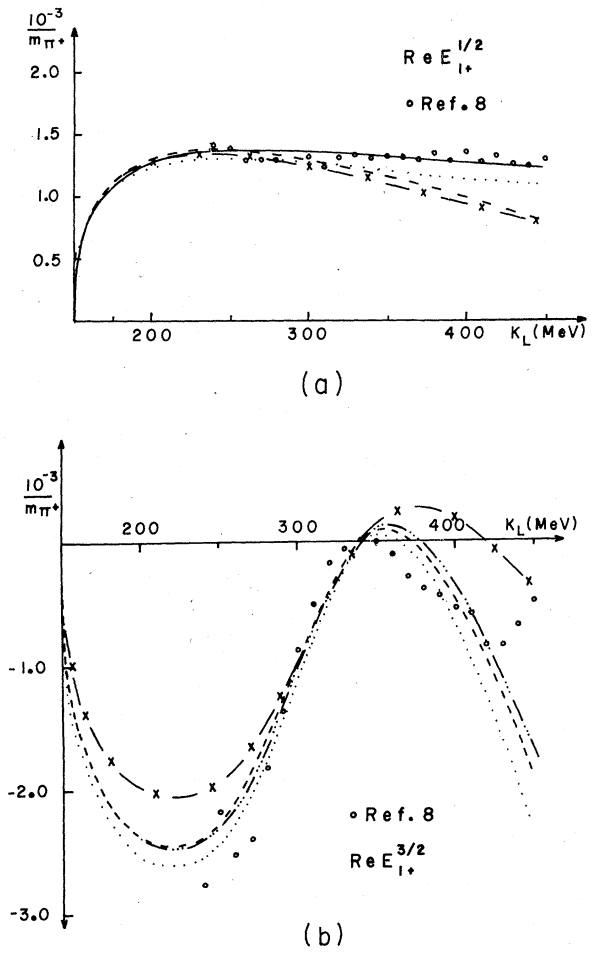

FIG. 3. (a) The real part of $E_{1+}^{1/2}$; (b) The real part of $E_{1+}^{3/2}$. The convention for the lines is the same of that in Fig. 1. For $E_{1+}^{1/2}$ the difference between solutions A, C, and D is negligible and is not shown. For $E_{1+}^{3/2}$ the input is zero and the difference between solutions A and C is negligible and is not shown.

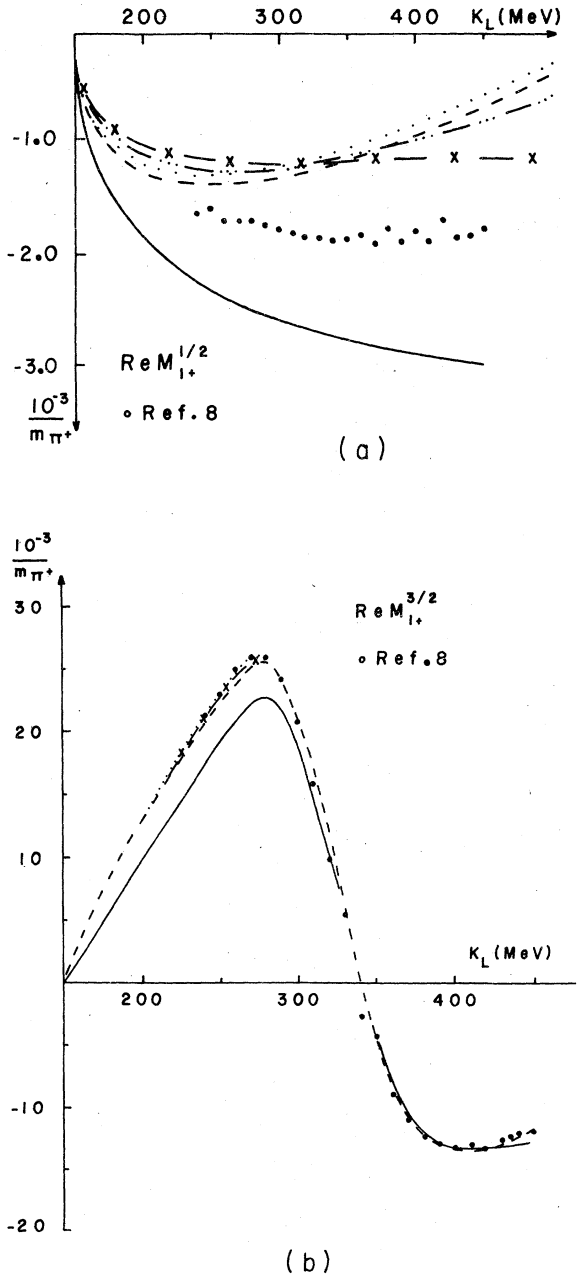

FIG. 4. (a) The real part of $M_{1+}^{1/2}$; (b) The real part of $M_{1+}^{3/2}$. The convention for the lines is the same of that in Fig. 1. For $M_{1+}^{1/2}$ the difference between solutions C and D is negligible and is not shown. For $M_{1+}^{3/2}$ the difference between solutions A, C, and D is negligible and is not shown.

sections on a proton target which is polarized parallel or antiparallel to the direction defined by $\vec{q}\times\vec{k}$:

$$T(\theta)=\frac{q}{k}\frac{1}{\sigma(\theta)}\,\mathrm{Im}(H_1H_2^*+H_3H_4^*). \tag{2.6}$$

In the region of the first resonance, it is more convenient to work with the magnetic and electric multipoles instead of the partial-wave helicity amplitudes. Therefore, we expand the H's directly in multipoles:

$$H_1=\frac{1}{\sqrt{2}}\cos\tfrac{1}{2}\theta\sin\theta \times\sum(E_{l+}-M_{l+}-E_{(l+1)-}-M_{(l+1)-})(P_l''-P_{l+1}''), \tag{2.7}$$

$$H_2=\frac{1}{\sqrt{2}}\cos\tfrac{1}{2}\theta \times\sum[(l+2)E_{l+}+lM_l+lE_{(l+1)-}-(l+2)M_{(l+1)-}] \times(P_l'-P_{l+1}'), \tag{2.8}$$

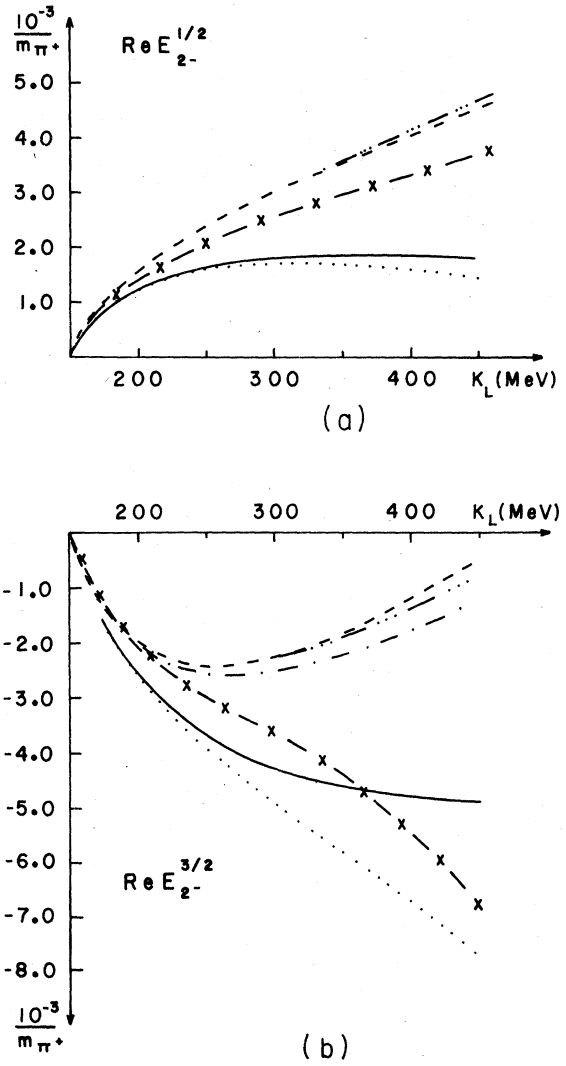

FIG. 5. (a) The real part of $E_{2-}^{1/2}$; (b) The real part of $E_{2-}^{3/2}$. The convention for lines is the same of that in Fig. 1. For $E_{2-}^{1/2}$ the difference between solutions A and C is negligible and is not shown.

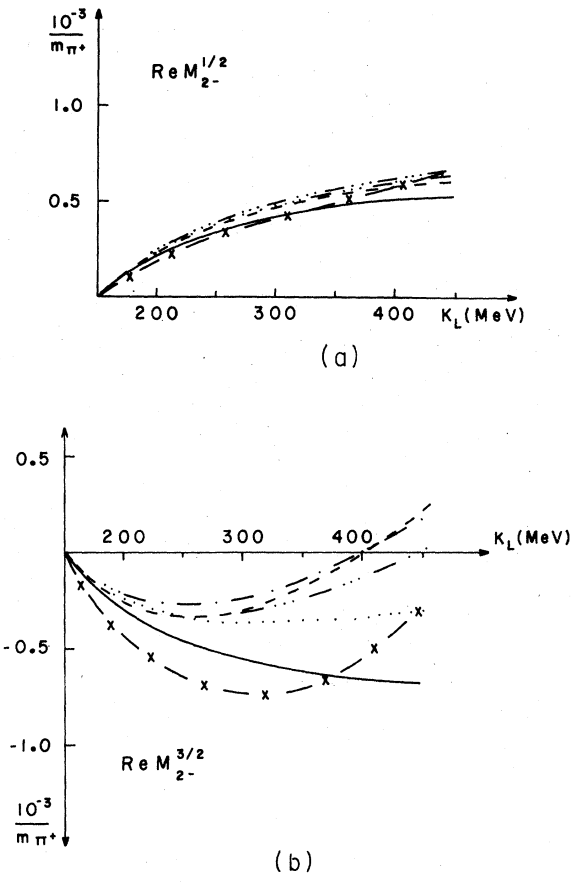

FIG. 6. (a) The real part of $M_{2-}^{1/2}$; (b) The real part of $M_{2-}^{3/2}$. The convention for the lines is the same of that in Fig. 1.

$$H_3=\frac{1}{\sqrt{2}}\sin^{\frac{1}{2}}\theta\sin\theta \times\sum(E_{l+}-M_{l+}+E_{(l+1)-}+M_{(l+1)-})(P_l''+P_{l+1}''), \quad (2.9)$$

$$H_4=\frac{1}{\sqrt{2}}\sin^{\frac{1}{2}}\theta \times\sum[(l+2)E_{l+}+lM_{l+}-lE_{(l+1)-}+(l+2)M_{(l+1)-}] \times(P_l'+P_{l+1}'). \quad (2.10)$$

In order to use the Fermi-Watson theorem, we will write the two amplitudes H^{π^+} and H^{π^0}, for π^+ and π^0 production, in terms of the amplitudes $H^{3/2}$ and $H^{1/2}$ for transition to the $I=\frac{3}{2}$ and $I=\frac{1}{2}$ final isotopic-spin states. Following the normalization of Berends and Weaver,[6] we have

$$H^{\pi^+}=\sqrt{2}\,(H^{1/2}-\tfrac{1}{3}H^{3/2}),$$
$$H^{\pi^0}=H^{1/2}+\tfrac{2}{3}H^{3/2}. \quad (2.11)$$

III. THE METHOD

In this section, we present a method for the determination of the multipoles. We call $M_{l\pm}^I$ and $E_{l\pm}^I$ the magnetic and electric multipoles leading to a final state with isotopic spin I, orbital angular momentum l, and total angular momentum $j=l\pm\frac{1}{2}$. In what follows, we use the generic symbol $h_{l\pm}^I$ to denote either $M_{l\pm}^I$ or $E_{l\pm}^I$. The method we have

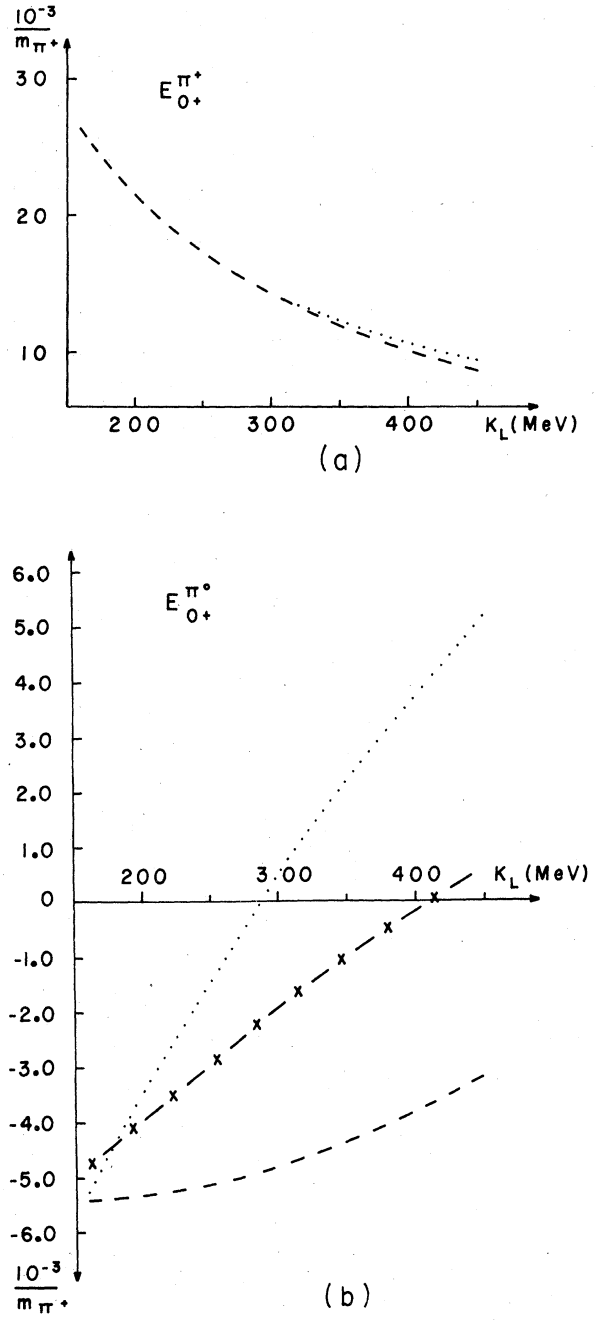

FIG. 7. (a) The real part of $E^{\pi^+}_{0+}$; (b) The real part of $E^{\pi^0}_{0+}$. The dashed line, the dotted line, and the —×— line correspond to solutions A, B, and E, respectively. For $E^{\pi^+}_{0+}$ the difference between solutions A and E is negligible and is not shown.

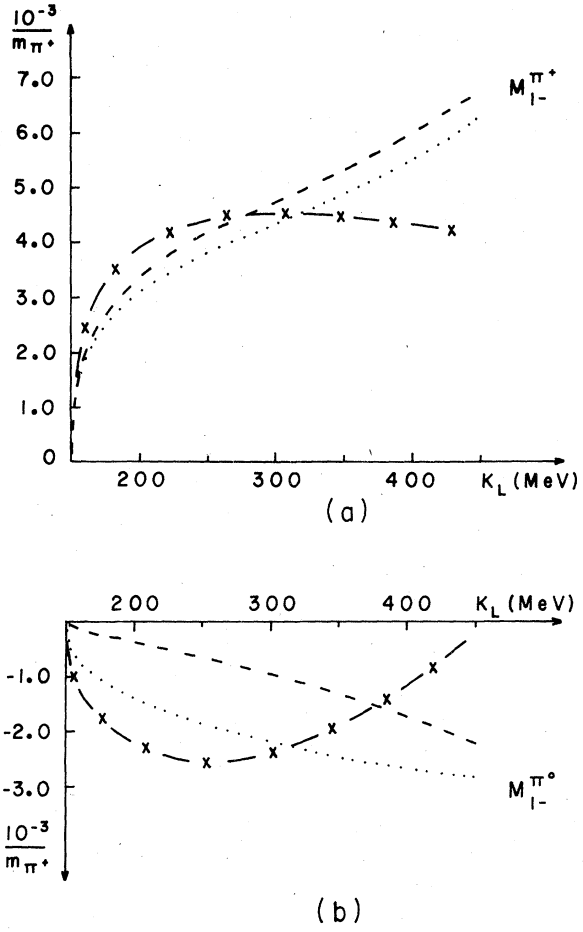

FIG. 8. (a) The real part of $M^{\pi^+}_{1-}$; (b) The real part of $M^{\pi^0}_{1-}$. The convention for the lines is the same of that in Fig. 7.

used is based in the following considerations:

(i) The most important feature in this region of energies is the excitation of the first π-N resonance;

(ii) π^0 photoproduction can be understood in terms of low angular momenta only, but this is not true for π^+ production where a forward peak in the differential cross section is already present at energies as low as $k_{\text{lab}} \simeq 300$ MeV;

(iii) Because of the Fermi-Watson theorem, the phase $\delta^I_{l\pm}$ of the multipoles $h^I_{l\pm}$ are the same as the corresponding π-N scattering amplitudes below the threshold for production of two pions. As the inelasticity in π-N scattering is, in this range, small, we extend the validity of the Fermi-Watson theorem[12] up to $k_{\text{lab}} \simeq 450$ MeV;

(iv) Theoretical models using dispersion-relation techniques have been presented in the literature. It is found that the main features of the data can be explained reasonably well through the Born terms and a resonant magnetic amplitude.

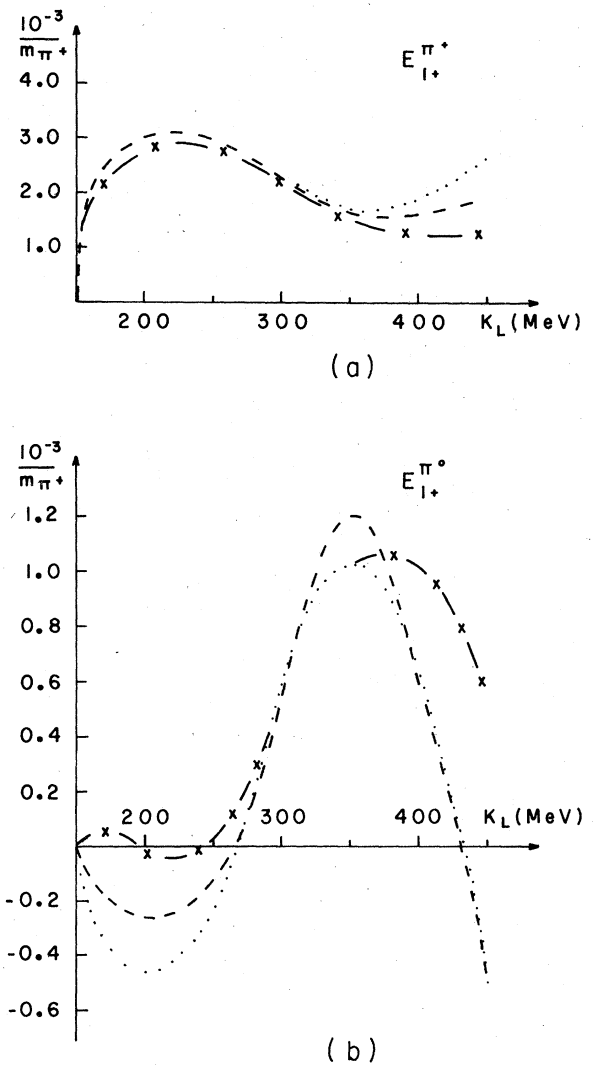

FIG. 9. (a) The real part of $E_{1+}^{\pi^+}$; (b) The real part of $E_{1+}^{\pi^0}$. The convention for the lines is the same of that in Fig. 7.

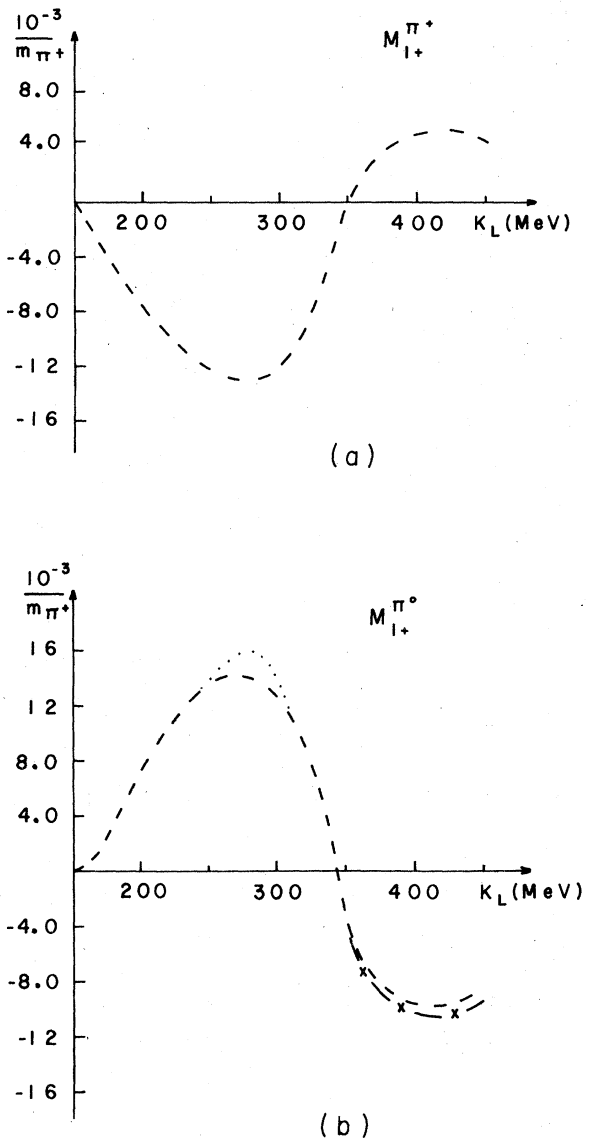

FIG. 10. (a) The real part of $M_{1+}^{\pi^+}$; (b) The real part of $M_{1+}^{\pi^0}$. The convention for the lines is the same of that in Fig. 7. For $M_{1+}^{\pi^+}$ the difference between solutions A, B, and E is negligible and is not shown.

Taking into account the above considerations, we assume that the multipoles are given by the sum of two terms: $h_{l\pm}^I$(input) and $\Delta h_{l\pm}^I$(correction). For all nonresonant amplitudes, $h_{l\pm}^I$(input) is given by the Born contribution corrected for absorption[16]:

$$h_{l\pm}^I(\text{input}) = (\text{Born contribution}) \times \exp(i\delta_{l\pm}^I)\cos\delta_{l\pm}^I. \tag{3.1}$$

The resonant amplitudes are taken as those given by Chew, Goldberger, Low, and Nambu[1]:

$$E_{1+}^{3/2}=0,$$
$$M_{1+}^{3/2}=\frac{\mu_p-\mu_n}{2}\frac{m_\pi}{f}\frac{k}{q^2}\exp(i\delta_{1+}^{3/2})\sin\delta_{1+}^{3/2}, \tag{3.2}$$

where $f^2\simeq 0.08$ and μ_p and μ_n are the total magnetic moments of proton and neutron.

The correction Δh is determined by a fit to the experimental data, and we assume that it is given by the product of three factors:

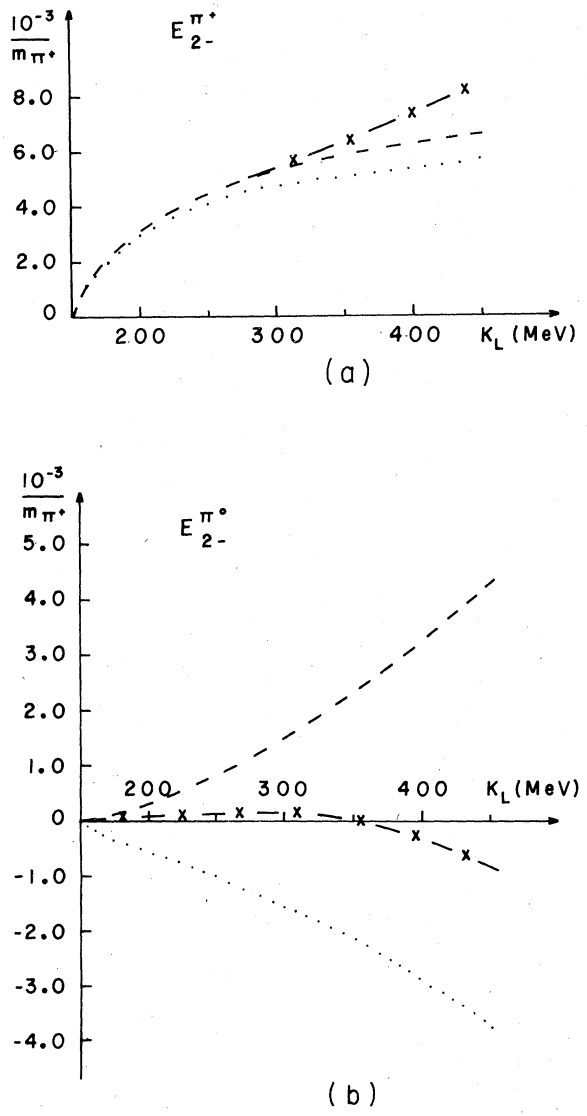

FIG. 11. (a) The real part of $E^{\pi^+}_{2-}$; (b) The real part of $E^{\pi^0}_{2-}$. The convention for the lines is the same of that in Fig. 7.

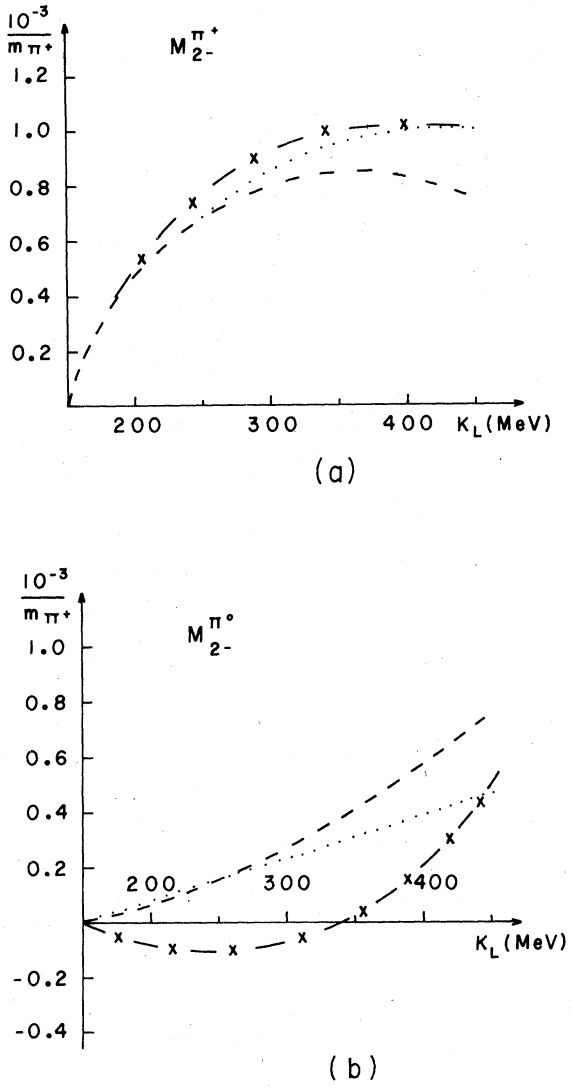

FIG. 12. (a) The real part of $M^{\pi^+}_{2-}$; (b) The real part of $M^{\pi^0}_{2-}$. The convention for the lines is the same of that in Fig. 7.

(i) $\exp(i\delta^I_{l\pm})$ which ensures the correct phase,

(ii) q^l which gives the correct threshold behavior, and

(iii) a second-degree polynomial in the center-of-mass energy ω which will introduce an extra energy dependence:

$$a^I_{l\pm}+\omega b^I_{l\pm}+\omega^2 c^I_{l\pm}. \tag{3.3}$$

The set of these 36 parameters is determined by searching, with the help of a computer, for a minimum of the function $\chi_w{}^2$ defined as

$$\chi_w{}^2=\frac{1}{N-n}\sum_{i=1}^{N} w_i\left(\frac{y^i_{\rm exp}-y^i_{\rm cal}}{\Delta y^i_{\rm exp}}\right)^2, \tag{3.4}$$

where N is the number of events i, n is the number of parameters, $y^i_{\rm exp}$, $\Delta y^i_{\rm exp}$, and $y^i_{\rm cal}$ are the experimental value, the corresponding experimental error, and the calculated value for one of the measurable quantities at a given angle and energy, and w_i is a weight factor which will be defined in the next section.

TABLE V. Multipoles for solution A. K_L is given in MeV and multipoles in units of $10^{-3}/m_{\pi+}$.

K_L	$E_{0+}^{1/2}$	$M_{1-}^{1/2}$	$E_{1+}^{1/2}$	$M_{1+}^{1/2}$	$E_{2-}^{1/2}$	$M_{2-}^{1/2}$	$E_{0+}^{3/2}$	$M_{1-}^{3/2}$	$E_{1+}^{3/2}$	$M_{1+}^{3/2}$	$E_{2-}^{3/2}$	$M_{2-}^{3/2}$
160	10.66	0.92	0.91	−0.79	0.57	0.08	−24.08	−1.63	−1.52	1.44	−0.79	−0.11
170	9.98	1.13	1.09	−0.97	0.87	0.12	−23.09	−2.03	−1.87	6.16	−1.19	−0.15
180	9.39	1.28	1.20	−1.10	1.14	0.17	−22.16	−2.33	−2.12	8.81	−1.51	−0.19
190	8.86	1.40	1.27	−1.19	1.38	0.21	−21.34	−2.58	−2.29	10.91	−1.76	−0.23
200	8.44	1.49	1.32	−1.26	1.59	0.24	−20.58	−2.79	−2.39	12.67	−1.96	−0.26
210	7.94	1.56	1.35	−1.31	1.78	0.27	−19.87	−2.97	−2.46	14.14	−2.12	−0.28
220	7.49	1.62	1.37	−1.34	1.96	0.30	−19.20	−3.13	−2.47	16.63	−2.23	−0.30
230	7.08	1.67	1.38	−1.37	2.12	0.33	−18.56	−3.28	−2.43	18.95	−2.31	−0.31
240	6.78	1.71	1.38	−1.38	2.26	0.35	−17.95	−3.44	−2.36	20.86	−2.37	−0.32
250	6.43	1.76	1.37	−1.38	2.40	0.38	−17.39	−3.58	−2.25	22.46	−2.40	−0.33
260	6.09	1.79	1.36	−1.38	2.54	0.40	−16.86	−3.72	−2.09	23.89	−2.40	−0.33
270	5.83	1.83	1.35	−1.37	2.66	0.42	−16.33	−3.86	−1.87	25.22	−2.39	−0.33
280	5.61	1.86	1.33	−1.36	2.78	0.44	−15.83	−4.00	−1.60	25.33	−2.36	−0.32
290	5.35	1.89	1.31	−1.34	2.90	0.45	−15.36	−4.15	−1.31	24.04	−2.32	−0.31
300	5.20	1.92	1.29	−1.32	3.01	0.47	−14.89	−4.29	−0.98	20.97	−2.26	−0.30
310	4.97	1.95	1.27	−1.29	3.12	0.49	−14.45	−4.44	−0.66	16.45	−2.19	−0.28
320	4.74	1.98	1.24	−1.26	3.23	0.50	−14.00	−4.60	−0.40	11.49	−2.11	−0.27
330	4.61	2.01	1.21	−1.23	3.34	0.51	−13.59	−4.75	−0.18	6.13	−2.02	−0.24
340	4.41	2.05	1.18	−1.19	3.44	0.52	−13.17	−4.92	−0.05	2.30	−1.92	−0.22
350	4.25	2.08	1.15	−1.15	3.54	0.54	−12.79	−5.08	0.08	−4.49	−1.82	−0.19
360	4.04	2.11	1.12	−1.11	3.65	0.55	−12.44	−5.26	0.08	−7.79	−1.70	−0.16
370	3.90	2.15	1.09	−1.07	3.75	0.56	−12.03	−5.44	0.02	−10.49	−1.59	−0.13
380	3.80	2.18	1.06	−1.03	3.86	0.56	−11.66	−5.61	−0.11	−12.14	−1.46	−0.09
390	3.69	2.22	1.03	−0.99	3.96	0.57	−11.32	−5.78	−0.28	−13.05	−1.33	−0.06
400	3.50	2.26	0.99	−0.93	4.06	0.58	−10.97	−6.01	−0.49	−13.23	−1.20	−0.02
410	3.35	2.31	0.95	−0.87	4.16	0.59	−10.65	−6.21	−0.73	−13.25	−1.06	0.03
420	3.22	2.35	0.92	−0.83	4.27	0.59	−10.34	−6.42	−1.00	−13.03	−0.91	0.07
430	3.12	2.40	0.88	−0.78	4.38	0.60	−10.03	−6.64	−1.29	−12.65	−0.77	0.12
440	3.05	2.44	0.85	−0.72	4.48	0.60	−9.71	−6.86	−1.61	−12.16	−0.62	0.17
450	3.01	2.49	0.81	−0.67	4.58	0.61	−9.37	−7.09	−1.93	−11.58	−0.47	0.22

IV. DATA ANALYSIS AND RESULTS

The experimental data for the photoproduction were taken from Menze, Pfeil, and Wilcke's data collection[17] which was published recently. The π-N phase shifts were taken from Almehed and Lovelace[18] analysis. Tables I, II, and III show the distribution of data among the measurable quantities and the distribution of data in intervals of energy and angle for three distinct sizes. Although the total number of data points used is quite large, the nonuniformity in distribution shown in Tables I, II, and III brings serious difficulties in the determination of the multipoles. To analyze these effects we considered the minimum of the χ_w^2 function, defined in the last section, in five different cases: A, B, C, D, and E.

In the first four cases we studied the effect of nonuniformity in the distribution of events in energy and angle, and in the last case we studied the effect of nonuniformity in the distribution of data through the eight measurable quantities: $\sigma(\theta)$, $P(\theta)$, $\Sigma(\theta)$, and $T(\theta)$ for final π^+'s and π^0's.

In cases A, B, C, and D we divided the experimental data sets $S_{\alpha\beta}^{+}$ ($S_{\alpha\beta}^{0}$) of events where a final π^+ (π^0) is produced having energy between $k_\alpha^{\rm lab}$ and $k_\alpha^{\rm lab}+\Delta k_\alpha^{\rm lab}$ and $\cos\theta$ between $\cos\theta_\beta$ and $\cos\theta_\beta+\Delta\cos\theta_\beta$ starting from $k_{\rm lab}=150$ MeV and $\cos\theta=-1$. In cases A, B, C, and D we put $(\Delta k^{\rm lab};\ \Delta\cos\theta)$ = (300 MeV; 2), (100 MeV; $\frac{1}{2}$), (60 MeV; $\frac{1}{3}$), and (50 MeV; $\frac{1}{4}$), respectively. Therefore, in cases A, B, C, and D we had 2, 24, 60, and 96 sets $S_{\alpha\beta}$. The weights w_i that appear in the expression (3.4) were set as

$$w_i=\frac{n}{n_i}, \tag{4.1}$$

TABLE VI. Multipoles for solution B. K_L is given in MeV and multipoles in units of $10^{-3}/m_{\pi+}$.

K_L	$E_{0+}^{1/2}$	$M_{1-}^{1/2}$	$E_{1+}^{1/2}$	$M_{1+}^{1/2}$	$E_{2-}^{1/2}$	$M_{2-}^{1/2}$	$E_{0+}^{3/2}$	$M_{1-}^{3/2}$	$E_{1+}^{3/2}$	$M_{1+}^{3/2}$	$E_{2-}^{3/2}$	$M_{2-}^{3/2}$
160	10.77	0.66	0.85	−0.75	0.47	0.08	−24.07	−2.11	−1.64	1.82	−0.95	−0.10
170	10.23	0.80	1.02	−0.92	0.71	0.13	−22.62	−2.64	−2.02	6.64	−1.47	−0.13
180	9.77	0.90	1.12	−1.04	0.91	0.17	−21.24	−3.03	−2.28	9.35	−1.92	−0.17
190	9.38	0.97	1.19	−1.12	1.07	0.21	−19.99	−3.35	−2.45	11.49	−2.30	−0.21
200	9.09	1.02	1.24	−1.18	1.20	0.24	−18.81	−3.62	−2.56	13.28	−2.64	−0.24
210	8.72	1.06	1.27	−1.23	1.31	0.27	−17.70	−3.85	−2.62	14.77	−2.95	−0.27
220	8.40	1.09	1.29	−1.26	1.41	0.30	−16.64	−4.05	−2.62	17.27	−3.22	−0.29
230	8.11	1.12	1.30	−1.27	1.48	0.33	−15.63	−4.23	−2.58	19.58	−3.47	−0.31
240	7.93	1.15	1.31	−1.28	1.54	0.36	−14.66	−4.40	−2.49	21.47	−3.71	−0.32
250	7.70	1.17	1.31	−1.28	1.59	0.38	−13.76	−4.56	−2.36	23.05	−3.93	−0.34
260	7.46	1.19	1.31	−1.28	1.63	0.41	−12.89	−4.71	−2.18	24.44	−4.13	−0.35
270	7.32	1.22	1.30	−1.26	1.66	0.43	−12.05	−4.85	−1.93	25.72	−4.33	−0.35
280	7.21	1.24	1.29	−1.25	1.68	0.45	−11.24	−4.99	−1.64	25.77	−4.52	−0.36
290	7.06	1.27	1.29	−1.23	1.69	0.47	−10.48	−5.12	−1.33	24.40	−4.70	−0.36
300	7.02	1.29	1.28	−1.20	1.70	0.48	−9.74	−5.25	−0.98	21.25	−4.88	−0.37
310	6.89	1.32	1.26	−1.17	1.70	0.50	−9.03	−5.38	−0.65	16.65	−5.06	−0.37
320	6.77	1.35	1.25	−1.14	1.70	0.52	−8.34	−5.52	−0.38	11.62	−5.24	−0.37
330	6.75	1.39	1.24	−1.11	1.70	0.53	−7.69	−5.64	−0.16	6.19	−5.41	−0.37
340	6.64	1.42	1.23	−1.07	1.69	0.54	−7.05	−5.78	−0.05	2.32	−5.59	−0.37
350	6.58	1.46	1.22	−1.03	1.68	0.56	−6.45	−5.91	0.06	−4.53	−5.77	−0.36
360	6.44	1.50	1.20	−0.99	1.66	0.57	−5.89	−6.05	0.03	−7.85	−5.95	−0.36
370	6.40	1.55	1.19	−0.94	1.65	0.58	−5.30	−6.18	−0.07	−10.55	−6.13	−0.36
380	6.41	1.60	1.18	−0.90	1.63	0.60	−4.75	−6.30	−0.24	−12.19	−6.32	−0.35
390	6.39	1.65	1.16	−0.86	1.61	0.61	−4.24	−6.42	−0.46	−13.08	−6.51	−0.35
400	6.26	1.70	1.14	−0.80	1.58	0.62	−3.73	−6.60	−0.70	−13.24	−6.71	−0.34
410	6.18	1.76	1.13	−0.75	1.55	0.63	−3.26	−6.75	−0.99	−13.22	−6.92	−0.33
420	6.12	1.82	1.12	−0.71	1.53	0.64	−2.81	−6.90	−1.30	−12.97	−7.12	−0.33
430	6.09	1.88	1.10	−0.66	1.50	0.65	−2.37	−7.05	−1.64	−12.55	−7.34	−0.32
440	6.11	1.95	1.09	−0.60	1.47	0.66	−1.94	−7.20	−2.00	−12.00	−7.56	−0.31
450	6.19	2.03	1.08	−0.55	1.44	0.66	−1.50	−7.37	−2.38	−11.38	−7.79	−0.31

where n is the total number of events divided by the number of sets, while n_i is the number of events in the set to which a given event i belongs. These weights should balance the importance of regions of energy and angle with unequal numbers of events in the calculation of the χ_w^2 function.

In case E we set

$$w_i = \left(\frac{N}{2n_i^\pi}\right)\left(\frac{N}{8m_i}\right), \tag{4.2}$$

where n_i^π is the number of π^+ (π^0) events according if the event i corresponds to a π^+ (π^0) in the final state and m_i is the number of events of a given kind of the eight measured quantities that we have analyzed (see Table I) to which the event i belongs. The first factor $(N/2n_i^\pi)$ is the same factor that appears in case A and would balance the importance of π^+ and π^0 events, the second factor $(N/8m_i)$ would balance the importance of the quantities $\sigma(\theta)$, $P(\theta)$, $\Sigma(\theta)$, and $T(\theta)$ in our analysis. We note that $w_i = 1$ if the distribution of events is uniform in all cases considered.

Of course the procedure we have used in the definition of the weights is quite arbitrary. Also, some of the values for n_i and m_i are quite small, and we should be careful in not giving them a statistical meaning. Our procedure, however, should provide an idea of the influence of distribution of data in energy and angle and among the different measurable quantities in the determination of the multipoles.

To save memory and computational time, the data were divided in intervals of energy 5 MeV. We look for a minimum of χ_w^2 letting the 36 parameters a's, b's, and c's vary. The results for χ_w^2 are given in Table IV and are of the same order in all cases.

TABLE VII. Multipoles for solution E. K_L is given in MeV and multipoles in units of $10^{-3}/m_{\pi+}$.

K_L	$E_{0+}^{1/2}$	$M_{1-}^{1/2}$	$E_{1+}^{1/2}$	$M_{1+}^{1/2}$	$E_{2-}^{1/2}$	$M_{2-}^{1/2}$	$E_{0+}^{3/2}$	$M_{1-}^{3/2}$	$E_{1+}^{3/2}$	$M_{1+}^{3/2}$	$E_{2-}^{3/2}$	$M_{2-}^{3/2}$
160	11.12	0.72	0.88	−0.63	0.53	0.07	−23.89	−3.06	−1.26	1.43	−0.78	−0.16
170	10.48	0.87	1.06	−0.77	0.81	0.11	−22.65	−3.79	−1.55	6.16	−1.20	−0.23
180	9.92	0.97	1.17	−0.87	1.05	0.14	−21.47	−4.31	−1.75	8.83	−1.55	−0.31
190	9.42	1.05	1.24	−0.94	1.25	0.18	−20.42	−4.71	−1.89	10.94	−1.82	−0.38
200	9.04	1.10	1.28	−1.00	1.44	0.21	−19.43	−5.01	−1.98	12.72	−2.07	−0.44
210	8.57	1.14	1.31	−1.04	1.60	0.23	−18.51	−5.24	−2.04	14.20	−2.29	−0.50
220	8.15	1.17	1.32	−1.07	1.74	0.26	−17.63	−5.41	−2.06	16.72	−2.48	−0.55
230	7.77	1.20	1.33	−1.09	1.88	0.28	−16.80	−5.54	−2.05	19.06	−2.65	−0.59
240	7.50	1.22	1.33	−1.11	2.00	0.31	−16.01	−5.64	−2.01	21.00	−2.81	−0.63
250	7.19	1.24	1.32	−1.12	2.10	0.33	−15.28	−5.69	−1.93	22.62	−2.95	−0.66
260	6.87	1.25	1.31	−1.13	2.21	0.35	−14.58	−5.72	−1.83	24.07	−3.09	−0.69
270	6.65	1.27	1.30	−1.14	2.30	0.37	−13.90	−5.72	−1.66	25.42	−3.23	−0.71
280	6.45	1.29	1.28	−1.14	2.39	0.38	−13.25	−5.70	−1.46	25.54	−3.36	−0.73
290	6.23	1.31	1.26	−1.14	2.48	0.40	−12.64	−5.66	−1.24	24.24	−3.50	−0.74
300	6.11	1.32	1.24	−1.14	2.57	0.42	−12.05	−5.60	−0.96	21.16	−3.64	−0.75
310	5.90	1.34	1.21	−1.14	2.65	0.44	−11.49	−5.52	−0.68	16.61	−3.78	−0.75
320	5.71	1.37	1.19	−1.14	2.73	0.45	−10.94	−5.43	−0.44	11.61	−3.94	−0.75
330	5.61	1.39	1.16	−1.14	2.80	0.47	−10.42	−5.32	−0.22	6.20	−4.09	−0.74
340	5.44	1.42	1.14	−1.13	2.88	0.49	−9.92	−5.20	−0.08	2.33	−4.26	−0.73
350	5.31	1.44	1.11	−1.13	2.96	0.50	−9.45	−5.06	0.14	−4.56	−4.43	−0.71
360	5.11	1.48	1.08	−1.12	3.03	0.52	−9.02	−4.93	0.22	−7.93	−4.62	−0.69
370	5.01	1.51	1.05	−1.12	3.11	0.54	−8.54	−4.76	0.27	−10.70	−4.82	−0.67
380	4.94	1.55	1.02	−1.12	3.19	0.55	−8.11	−4.58	0.27	−12.42	−5.03	−0.63
390	4.86	1.59	0.99	−1.12	3.26	0.57	−7.72	−4.38	0.24	−13.41	−5.25	−0.60
400	4.69	1.64	0.95	−1.11	3.34	0.59	−7.32	−4.22	0.17	−13.65	−5.48	−0.56
410	4.56	1.69	0.92	−1.10	3.42	0.60	−6.96	−4.03	0.09	−13.73	−5.73	−0.52
420	4.45	1.74	0.89	−1.11	3.50	0.62	−6.62	−3.82	−0.02	−13.57	−5.99	−0.47
430	4.37	1.79	0.85	−1.11	3.58	0.64	−6.28	−3.60	−0.13	−13.26	−6.27	−0.41
440	4.34	1.85	0.82	−1.11	3.66	0.66	−5.94	−3.38	−0.26	−12.83	−6.56	−0.36
450	4.34	1.92	0.78	−1.11	3.74	0.68	−5.60	−3.15	−0.40	−12.31	−6.87	−0.29

Figures 1 to 6 show the multipole solutions for cases A, B, C, D, and E. The graphs show that multipoles $M_{1-}^{1/2}$, $M_{1+}^{1/2}$, $M_{1+}^{3/2}$, $E_{1+}^{1/2}$, $E_{1+}^{3/2}$, and $M_{2-}^{1/2}$ are quite stable as we move from solution A to E, giving greater confidence in their determination. We can also notice that solutions A, C, and D are quite close for all multipoles. This is not true, in general for solutions B and E. To study the origin of these differences we have calculated the multipoles for final π^+ and π^0 states.

In Figs. 7 to 12 we show these multipoles results for solutions A, B, and E. One sees that the large differences appear for final π^0 and only for E_{0+}, M_{1-}, and E_{2-}. For final π^+ all the solutions for M_{1+} and E_{0+} multipoles almost coincide for all energies. For M_{1-}, E_{1+}, E_{2-}, and M_{2-} solutions differ for less than ~10% for energies up to 300 MeV. These differences increase when we go up to 450 MeV. These discrepancies may be due to the much poorer data in π^0 production which it is not being able to discriminate between independent solutions. Solution E tries to put on the same footing events coming from $\sigma(\theta)$, $P(\theta)$, $\Sigma(\theta)$, and $T(\theta)$. The differences between the number of events for these quantities are very large (see Table I). The number of experiments for T and P are very small; they are mostly in large energies and concentrated in angles from 50° to 120°. As the statistics are so poor, it is quite difficult to draw any conclusions from solution E. Of course, the discrepancies obtained are an indication that we do need better data for $P(\theta)$, $T(\theta)$, and $\Sigma(\theta)$.

Tables V, VI and VII list the numerical values obtained for the multipoles in cases A, B, and E.

In Figs. 1–6 we also show the values obtained by Berends and Donnachie.[8] We refer to their work for comparison with other authors. For the important multipole $M_{1+}^{3/2}$ our results are practical-

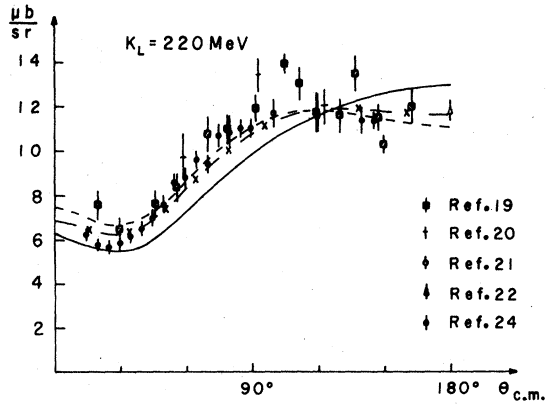

FIG. 13. Cross section for π^+ photoproduction at 220 MeV. The solid line is the input. The dashed line and the — × — line correspond to solutions A and E, respectively. The differences between solutions A, B, C, and D are small and are not shown.

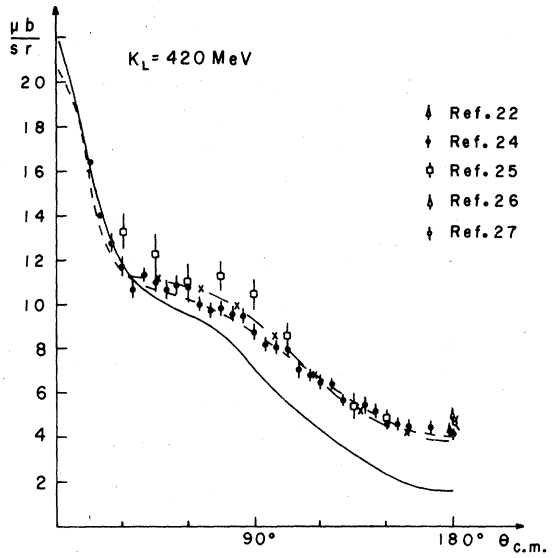

FIG. 15. Cross section for π^+ photoproduction at 420 MeV. The solid line is the input. The dashed line and the — × — line correspond to solutions A and E, respectively. The differences between solutions A, B, C, and D are small and are not shown.

ly the same. For the large multipoles the results of Ref. 8 are larger than ours, while for $M_{1-}^{1/2}$, $E_{1+}^{1/2}$, and $M_{1-}^{3/2}$ the differences are small.

In Figs. 13–18 we show our results for π^+ and π^0 differential cross section at three different energies. The curves show that all solutions give almost the same results for $\sigma(\theta)$ and they fit the data pretty well.

In Fig. 19 we plot $\Sigma(\theta)$ for π^+ and π^0 production at $K_{\text{lab}} = 330$ and 420 MeV, respectively. We see that, as for $\sigma(\theta)$, the curves for all solutions do not differ too much.

In Figs. 20 and 21 we show the final-nucleon po-

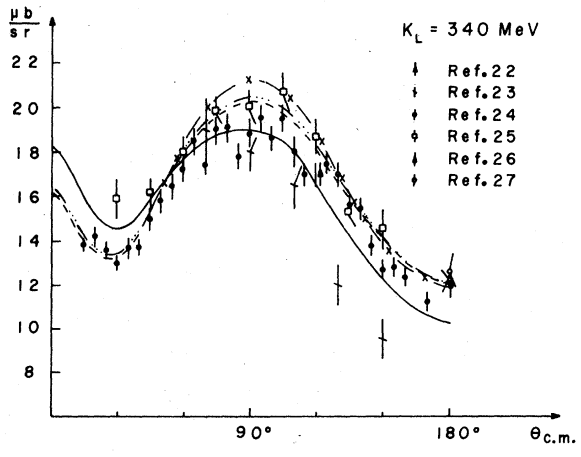

FIG. 14. Cross section for π^+ photoproduction at 340 MeV. The solid line is the input. The dashed line, the —···— line, and the — × — line correspond to solutions A, C, and E. respectively. The differences between solutions A, B, and D are small and are not shown.

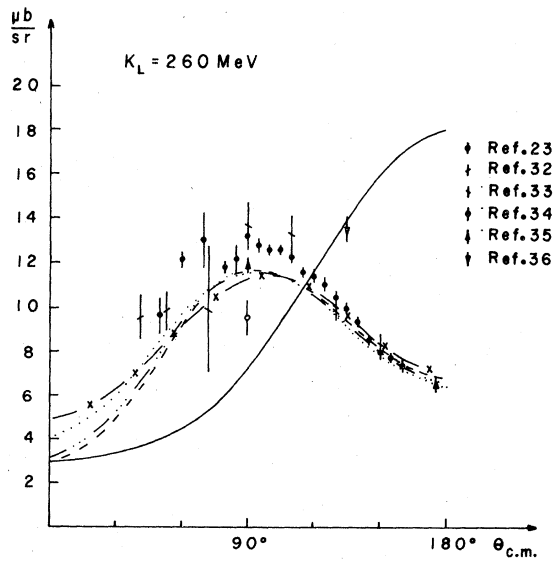

FIG. 16. Cross section for π^0 photoproduction at 260 MeV. The solid line is the input. The dashed line, the dotted line, the —··· — line, and the — × — correspond to solutions A, B, C, and E, respectively. The difference between solutions A and D is small and is not shown.

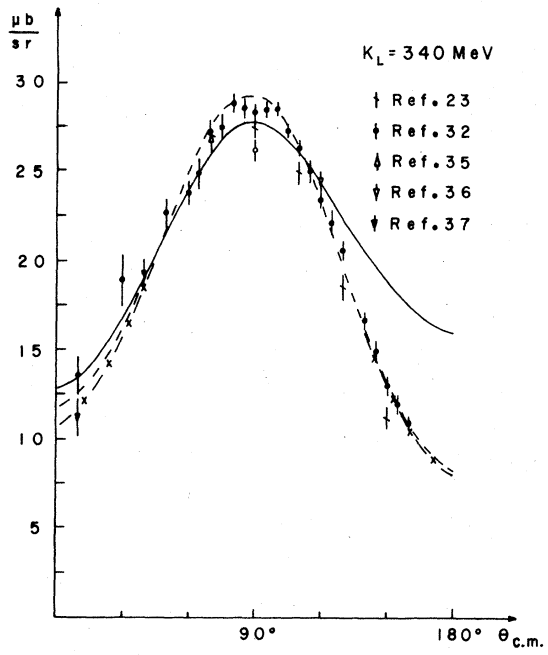

FIG. 17. Cross section for π^0 photoproduction at 340 MeV. The solid line is the input. The dashed line and the — × — line correspond to solutions A and E, respectively. The differences between solutions A, B, C, and D are small and are not shown.

larization, $P(\theta)$, and the polarized-target asymmetry $T(\theta)$ at high energies. As we expect, the π^+ results are almost the same for all solutions. For π^0 production, solutions A, B, and E show large differences at

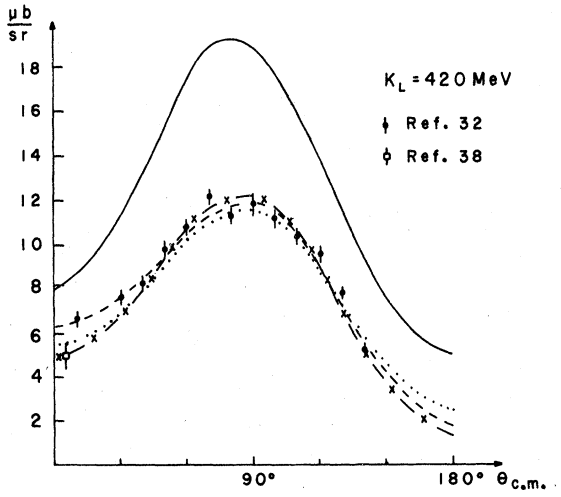

FIG. 18. Cross section for π^0 photoproduction at 420 MeV. The solid line is the input. The dashed line, the dotted line, and the — × — line correspond to solutions A, B, and E, respectively. The differences between solutions A, C, and D are small and are not shown.

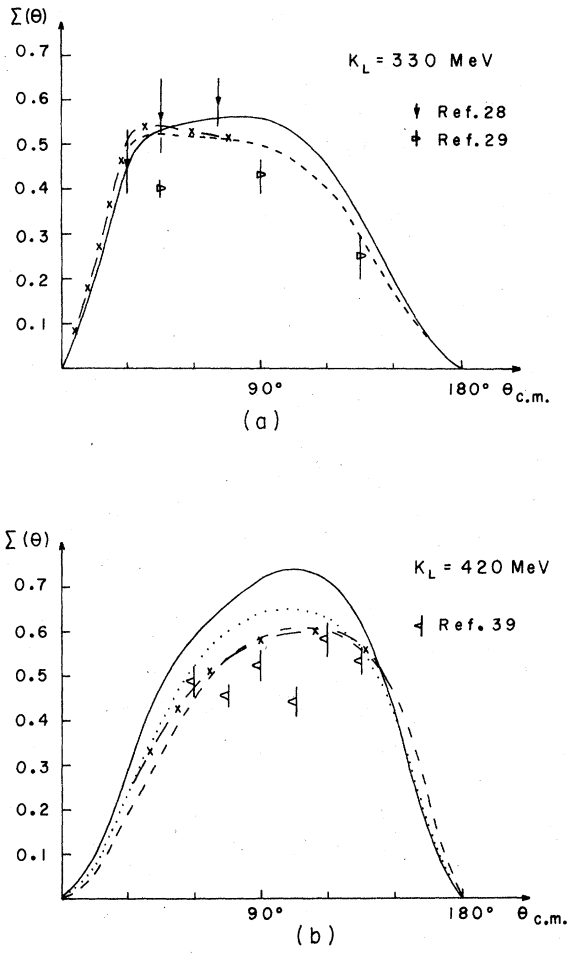

FIG. 19. (a) Photon asymmetry for π^+ photoproduction at 330 MeV. The solid line is the input. The dashed line and the —×— line correspond to solutions A and E, respectively. The differences between solutions A, B, C, and D are small and are not shown. (b) Photon asymmetry for π^0 photoproduction at 420 MeV. The solid line is the input. The dashed line, the dotted line, and the —×— line correspond to solutions A, B, and E, respectively. The differences between solutions A, C, and D are small and are not shown.

large and small angles. The experimental results, however, are not able to distinguish the best solution since they are concentrated around 90°.

Our results for χ_w^2 values and the fits in Figs. 13–21 show that, in order to distinguish between our solutions, we do need much more π^0 production data mainly for polarized-target experiments and final-nucleon-polarization experiments at small and large angles.

From our analysis and the comparison with Ref. 8 we believe that the multipoles $M_{1-}^{1/2}$, $M_{1+}^{1/2}$, $M_{1+}^{3/2}$,

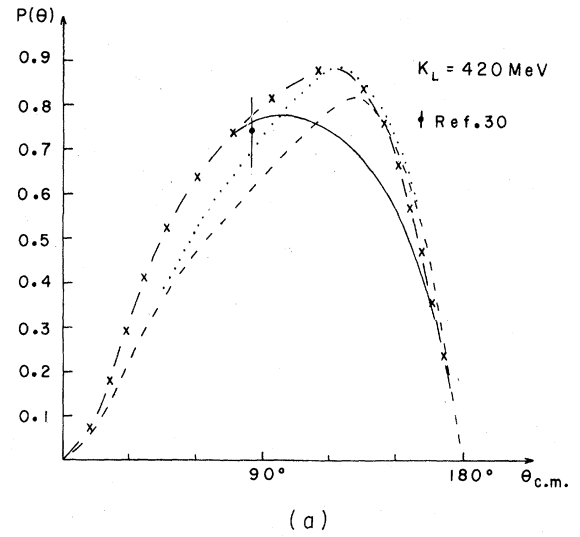

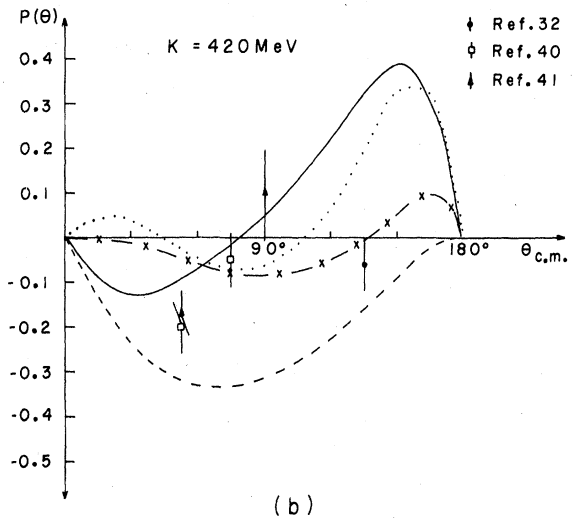

FIG. 20. Recoil-nucleon polarization at 420 MeV. The solid line is the input. The dashed line, the dotted line, and the — × — line correspond to solutions A, B, and E, respectively. The differences between solutions A, C, and D are small and are not shown. (a) π^+ photoproduction; (b) π^0 photoproduction.

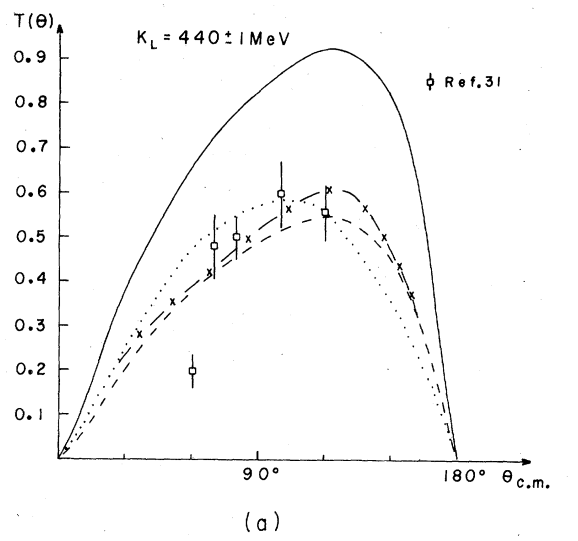

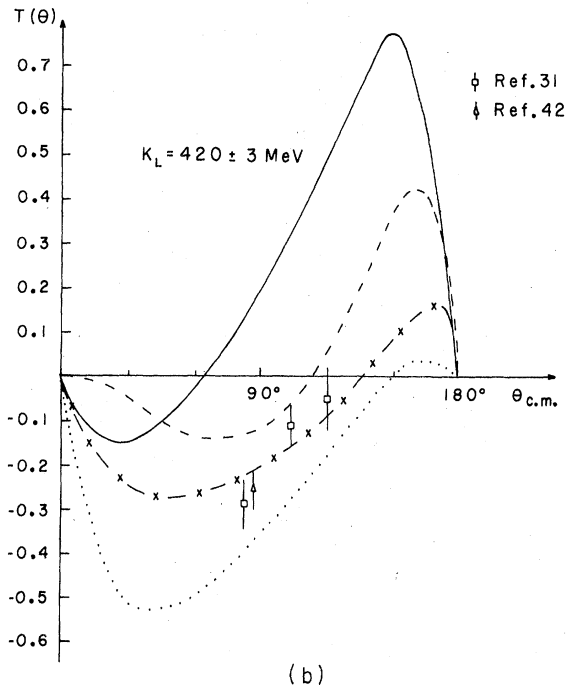

FIG. 21. Polarized-target asymmetry. The solid line is the input. The dashed line, the dotted line, and the — × — line correspond to solutions A, B, and E, respectively. The differences between solutions A, C, and D are small and are not shown. (a) π^+ photoproduction at 440 MeV; (b) π^0 photoproduction at 420 MeV.

$E_{1+}^{1/2}$, $E_{1+}^{3/2}$, $M_{2-}^{1/2}$ for final isotopic-spin states can be considered reasonably well determined. In fact all solutions including solution E are practically the same. For the other multipoles, the combinations for final π^+ states have solutions that are much closer than for final π^0 states, as we can see in Figs. 7–12.

We hope that when more data are available, mainly for final-nucleon polarization and polarized-target asymmetry, the above uncertainties can be solved.

[1]G. F. Chew, M. L. Goldberger, F. E. Low, and Y. Nambu, Phys. Rev. 106, 1345 (1957).
[2]M. Nigro and E. Schiavuta, Nuovo Cimento 50, 358 (1967).
[3]R. L. Walker, Phys. Rev. 182, 1729 (1969).
[4]Yu. M. Aleksandrov, V. K. Grushin, and E. M. Leikin, Nucl. Phys. B10, 145 (1969).
[5]P. Noelle, W. Pfeil, and D. Schwela, Nucl. Phys. B26, 461 (1971).
[6]F. A. Berends and D. L. Weaver, Nucl. Phys. B30, 575 (1971).
[7]J. R. Rios Leite and N. Zagury, Rev. Bras. Fis. 4, 191 (1974).
[8]F. A. Berends and A. Donnachie, Nucl. Phys. B84, 342 (1975).
[9]R. G. Moorhouse, H. Oberlack, and A. H. Rosenfeld, Phys. Rev. D 9, 1 (1974).
[10]W. J. Metcalf and R. L. Walker, Nucl. Phys. B76, 253 (1974).
[11]R. C. E. Devenish, D. H. Lyth, and W. A. Rankin, in *Proceedings of the XVII International Conference on High-Energy Physics, London*, 1974, edited by J. R. Smith (Rutherford Laboratory, Chilton, Didcot, Berkshire, England, 1974).
[12]K. Watson, Phys. Rev. 95, 228 (1954); E. Fermi, Suppl. Nuovo Cimento 2, 58 (1955).
[13]M. Jacob and C. Wick, Ann. Phys. (N.Y.) 7, 404 (1959).
[14]S. D. Ecklund and R. L. Walker, Phys. Rev. 159, 1195 (1967).
[15]See, for example, W. Schmidt and G. Schwiderski, Kernforschungszentrum, Karlsruhe report, 1966 (unpublished).
[16]See, for example, M. L. Goldberger and K. M. Watson, *Collision Theory* (Wiley, New York, 1964), p. 547.
[17]D. Menze, W. Pfeil, and R. Wilcke, Bonn University report, 1977 (unpublished).
[18]S. Almehed and C. Lovelace, Nucl. Phys. B40, 157 (1972).
[19]M. I. Adamovich *et al.*, Yad. Fiz. 7, 579 (1968) [Sov. J. Nucl. Phys. 7, 360 (1968)].
[20]M. Beneventano *et al.*, Nuovo Cimento 4, 323 (1956).
[21]D. W. G. S. Leith *et al.*, Phys. Lett. 8, 355 (1964).
[22]J. P. Pahin *et al.*, Phys. Rev. Lett. 27, 1244 (1971).
[23]R. W. Clifft *et al.*, Phys. Rev. Lett. 33, 1500 (1974).
[24]G. Fischer *et al.*, Nucl. Phys. B16, 119 (1970).
[25]T. Fujii *et al.*, Tokyo report, 1976 (unpublished).
[26]H. W. Dannhausen *et al.*, Bonn University report, 1975 (unpublished).
[27]I. Endo, thesis, Tokyo, 1970 (unpublished).
[28]M. Grilli *et al.*, Nuovo Cimento 54, 877 (1968).
[29]F. F. Lin *et al.*, Phys. Rev. 136, B1183 (1964).
[30]M. Hahn *et al.*, Bonn University report, 1971 (unpublished).
[31]M. Fukushima *et al.*, Nagoya report, 1977 (unpublished).
[32]H. Genzel *et al.*, Z. Phys. 268, 19 (1974).
[33]W. S. MacDonald *et al.*, Phys. Rev. 107, 577 (1957).
[34]D. B. Miller *et al.*, Proc. Phys. Soc. (London) 81, 343 (1963).
[35]R. Morand *et al.*, Phys. Rev. 180, 1299 (1969).
[36]P. Dougan *et al.*, Z. Phys. A276, 155 (1976).
[37]V. L. Highland *et al.*, Phys. Rev. 132, 1293 (1963).
[38]Y. Hemmi *et al.*, Phys. Lett. B43, 79 (1973).
[39]V. B. Ganenko *et al.*, contribution to the 1975 International Symposium on Lepton and Photon Interactions at High Energies, Stanford, California, 1975 (unpublished).
[40]D. Trines, thesis, Bonn University, 1972, PIB 1–160 (unpublished).
[41]K. H. Althoff *et al.*, Phys. Lett. B26, 677 (1968).
[42]P. Feller *et al.*, Phys. Lett. B55, 241 (1975).